City Research Online

City, University of London Institutional Repository

This is the accepted version of the paper.

This version of the publication may differ from the final published version.

Carbon Nano Bowls Filled with MoS$_2$ Nanosheets as Electrode Materials for Supercapacitors

Lijian Wang [a], Fenghua Liu [a], Binyuan Zhao [a, *], Yuesheng Ning [a], Lifeng Zhang [b, *], Robert Bradley [c, d, e] and Weiping Wu [f,*]

[a] State Key Laboratory of Metal Matrix Composites, School of Materials Science and Engineering, Shanghai Jiao Tong University, Shanghai, 200240, China

[b] School of Materials Science and Engineering, Shaanxi University of Science and Technology, Xi'an 710021, Shaanxi, China

[c] Department of Materials, University of Oxford, 16 Parks Road, Oxford, OX1 3PH, United Kingdom

[d] MatSurf Ltd, The Old Stables Marion Lodge, Little Salkeld, Penrith, Cumbria, CA10 1NW, United Kingdom

[e] School of Energy Resources, University of Wyoming, Laramie, WY, 82071, USA

[f] Department of Electrical and Electronic Engineering, School of Mathematics, Computer Science and Engineering, City, University of London, Northampton Square, London, EC1V 0HB, United Kingdom

ABSTRACT

Simultaneously achieving high gravimetric capacitance and volumetric capacitance remains as a major challenge in the development of supercapacitor electrode materials. A class of hollow carbon nano bowls (HCNBs) with a unique semi-concave geometry has been synthesized by a facile template method. The HCNBs can serve as a nanoreactor for the in-situ space-confined growth of ultra-small size, few layer two-dimensional (2D) molybdenum disulfide (MoS_2) nanosheets. When used as the electrode materials for supercapacitors, the MoS_2 nanosheets inside HCNBs named MoS_2@HCNBs demonstrated outstanding gravimetric capacitance (560 F g^{-1} at 0.2 A g^{-1}) and volumetric capacitance (874 F cm^{-3}) at the same time. The cycling performance of MoS_2@HCNBs (94.4% capacitance retention after 5000 cycles) is also much higher than HCNB@MoS_2 in which the surfaces of HCNBs were covered by the 2D MoS_2 nanosheets. Several factors have been leading to the boosted performances and the mechanisms have been analyzed. The HCNBs with high surface area, developed porosity and ultrathin carbon shells promote the rapid electrolyte penetration and provide a conductive pathway for excellent ion and electron transport. The ultra-small few layer MoS_2 nanosheets inside the HCNBs help to induce extra electrochemical double-layer capacitance as well as higher pseudocapacitance. More importantly, the semi-concave HCNBs can protect the structural stability of MoS_2 nanosheets and contribute an enhanced packing density to further improve the volumetric capacitance of the hybrid MoS_2@HCNBs.

KEYWORDS: supercapacitors, molybdenum disulfide MoS_2, carbon nano bowls, gravimetric capacitance, volumetric capacitance

INTRODUCTION

Supercapacitor is an important energy storage technology for the current and future's industry and society. It represents one of the most promising solutions, due to its fast charge and discharge rate, long cycle life, high power density and low cost[1]. The exploration of new electrode materials with superior performances is critical to solve energy conversion and storage challenges. Massive differences on the performances of the two classes of supercapacitor materials have been observed. There are two energy storage mechanisms of supercapacitors, Electrochemical Double Layer Capacitance (EDLC) and Pseudocapacitance (PC). Unlike the EDLC which involves no chemical reaction but only the reversible ion adsorption/desorption, the pseudocapacitive materials such as Ruthenium(IV) oxide RuO_2 store energy faradaically via the reduction-oxidation reactions of the active material on the electrode[2]. By combining the two mechanisms, a higher overall performance could be achieved[3]. However, achieving high gravimetric capacitance and volumetric capacitance of supercapacitors while maintaining excellent cycle stability, has been the bottleneck that limits the rapid development and broader applications of supercapacitors[4].

Porous carbon, graphene and two-dimensional (2D) transition metal dichalcogenide (TMDCs), such as molybdenum disulfide (MoS_2) and tungsten disulfide (WS_2), have been extensively studied in the field of optoelectronics[5, 6], photovoltaics[7], rechargeable lithium batteries[8 9, 10], solar thermal energy harvest[11, 12, 13], Joule heaters[14] and so on. Recently, the 2D layered graphene[15] and the TMDC materials[9] have been studied as a new class of electrode materials for supercapacitors[8 16, 17], along with the 0D (carbon nano onions), 1D (carbon nanotubes) and 3D carbon (active carbon, mesoporous carbon) as supercapacitor electrode materials. MoS_2 based supercapacitor can store electrical energy via three different mechanisms[16]. Besides the EDLC

and the pseudocapacitive capacitor (contributed by the redox reaction of Mo atoms), the larger spacing of 2D MoS₂ layers can accelerate the rapid reversible intercalation of electrolyte ions (H^+, K^+, NH_4^+) between layers, which can contribute a part of the embedded pseudocapacitance.

However, the conductivity of semiconducting 2H-phase and 3R-phase of MoS₂ is much lower than that of carbon materials[18]. Although the 1-T phase MoS₂ whose conductivity (10–100 S cm⁻¹) is metallic[19], its conductivity is one magnitude lower than carbon materials (1000 S cm⁻¹ or higher)[20]. Besides, the 1-T phase is metastable, much more difficult and expensive to synthesize, and the conductivity remains as a limiting factor for higher performance supercapacitor devices. In addition, the highly stacked MoS₂ sheets make the inter-layer sites active for ion insertions be limited, which hinders the full exertion of its theoretical capacity. Therefore, most supercapacitors with MoS₂ electrodes reported so far, demonstrated relatively low gravimetric capacitance (150-700 F g⁻¹)[21] [22] or volumetric capacitance (100-700 F cm⁻³)[23] [19].

In order to overcome these challenges, different strategies such as doping, intercalations or hybridizing with other materials with better conductivity, have been proposed to improve their electrochemical performances[24]. Hybridizing MoS₂ with carbon is one of the most effective approaches, as it can significantly enhance the conductivity and the specific surface area of the MoS₂ based electrodes[25]. Particularly, hollow carbon is an interesting class of carbon material[26], due to its unique geometry, large specific area, large interior void, low densities, high electrical conductivity, as well as its mechanical and thermal stability. The hollow and core-shell structures can also effectively increase the electrolyte/electrode contact area, reduce the diffusion distance of the ions in the electrolyte[27] and effectively suppress electrochemical oxidation reactions[28], so that the cycle stability of the supercapacitor device could be improved. In the previous studies, it has been known that it's easier to fill inorganic nano materials into large voids (tens to hundreds

nm) of hollow carbon spheres. It is possible but difficult to fill materials into the ultra-small spaces in carbon nanotubes. So far, there are very few reports or effective methods to generated meso sized (especially from 2 nm to 10 nm) cavities that can be used for space confined growth of 2D materials in hollow carbon structures.

Although the reported MoS_2-nano carbon composites could help to improve the conductivity and specific capacitance, the enhancement of electrochemical performances is still insufficient for many practical applications. For instance, when the semiconducting 2D MoS_2 with poor conductivity covers the surface of carbon spheres, the connection between the carbon and MoS_2 becomes weak, especially at high current densities. In addition, the MoS_2 nano flakes or nano clusters on the carbon surface are still thick (usually ≥20 nm) and are directly exposed to the electrolyte, this configuration is less stable during cycling at high current density[29]. To date, there is little understanding on the space confined growth of 2D MoS_2, or the impact of the topology of the MoS_2-carbon hybrid materials on the supercapacitor performances. Therefore, it is important to synthesize materials with optimized structures but in different architectures, so that the synergistic effect of carbon materials and MoS_2 can be clearly understood and fully utilized in supercapacitor devices.

In this study, a facile in-situ space-confined template synthesis method for the 2D MoS_2-carbon hybrid materials has been developed. Three different materials for supercapacitor electrodes were successfully prepared, the Hollow Carbon Nano Bowls (HCNBs), the MoS_2@HCNB (ultrathin 2D MoS_2 nanosheets confined inside the cavity of the HCNBs) and the HCNB@MoS_2 with thick MoS_2 nano flakes grown on the surface of HCNB. The synthetic method utilized the SiO_2 as the first template to obtain the HCNBs, the obtained carbon nano bowls were used as nano reactor and the succeeding second templates. By controlling the

synergistic effect between shell thickness and pore structure in the carbon layer, the original spherical structure of SiO_2@C can be controllably transferred into carbon nano spherical bowls with semi-concave geometry. Then, the ammonium thiomolybdate solution ((NH_4)$_2MoS_4$) was impregnated into HCNB by vacuum incipient wetness method followed by calcination to prepare MoS_2@HCNB.

RESULTS and DISCUSSION

The new nanoscale architectures, combines several advantages as supercapacitor electrodes: (1) The carbon material HCNB provides high surface areas, hierarchical porous structures, high electrical conductivity, high nitrogen (N) atoms and oxygen (O) atomic doping, beneficial to acquire the high capacitance, good rate capability and cycling stability; (2) Monolayer and few layer 2D MoS_2 nanosheets is confined to grow inside the cavity of hollow HCNB, and 2D MoS_2 nanosheets are enfolded and protected by thinner carbon shell could avoid the direct exposure to the electrolytes, which can effectively overcome the poor cycle stability of pseudocapacitive electrode materials; (3) Monolayer and few layer of 2D MoS_2 nanosheets possess a large number of active sites, shortening the diffusion distance of ions, which is beneficial to the storage of ions and transfer of ions/electrons[30]; (4) compared to hollow carbon spheres, the HCNB with semi-concaves, bowl shaped structure has a smaller void volume and the semi-concaves structure by stacking two layers of curved carbon films. The distance between the upper and lower carbon layers is significantly reduced, which could encapsulation the appropriate amount of 2D MoS_2 nanosheets. Meanwhile, MoS_2 could be directly connected to the upper and lower carbon shells to improve the electrolyte ions between carbon-MoS_2-carbon. This can overcome the difficult that pseudocapacitive electrode material is uneasy to fully exert due to the agglomeration and stacking. The synthesized novel MoS_2@HCNB demonstrated excellent gravimetric capacitance

of 560 F g^{-1} (with the volumetric capacitance as high as 874 F cm^{-3}). Furthermore, excellent cycling performance (94.4% capacitance retention after 5000 cycles) for supercapacitors has been achieved by using such an electrode material.

Synthesis of MoS$_2$@HCNB and HCNB@MoS$_2$

The template method has been used to obtain the MoS$_2$@HCNB, the synthesis steps are shown in **Scheme 1(I)**. Simply by changing the ratio between carbon precursors and tetraethyl orthosilicate (TEOS), the structures of the obtained hollow carbon materials can be controllably tuned from nano hollow spheres to nano bowls. Firstly, a layer of resorcinol-formaldehyde polymer doped with small SiO$_2$ spheres (diameter, 190±10nm), is coated by a one-pot polymerization on the surface of Silica (SiO$_2$) spheres. Ethylenediamine (EDA), a catalyst for both the polymerization and tetraethyl orthosilicate (TEOS) hydrolysis, was also used as nitrogen (N) precursor for in-situ N doping in carbon materials. After calcination and removal of the SiO$_2$ (both the SiO$_2$ spheres and small SiO$_2$ particles intertwined within the outer carbon layers), the thinner porous carbon shells could not maintain the original spherical three-dimensional structure during the SiO$_2$ removal process and then like a deflated ball, they collapse slowly inward to form a bowl-like structure, the HCNBs with semi-concaved bowl shape was prepared.

i) For the **MoS$_2$@HCNB**, the ammonium thiomolybdate solution was adsorbed into the HCNB by vacuum incipient wetness method. The HCNB with semi-concaves could act as a nanoreactor. Pure HCNB with a hollow internal cavity structure has a high specific surface area (1400 m^2 g^{-1}) and an average pore size of 2.25 nm, this suggests that the driving force behind the filling of the hollow core of the carbon capsules by the inorganic compound solution is the capillary motion through the mesopores of the carbon shell during vacuum incipient wetness process. Similarly, its high specific surface area and dispersed pore structure distribution allow MoS$_2$ to grow

through more active sites within HCNB. Then, the surface of HCNB was rinsed by rapid suction filtration of ethanol to remove the $(NH_4)_2MoS_4$ precursor remaining on the surface of HCNB. This ensures that MoS_2 will not grow on the outer surface of the HCNB. After the annealing process, the ultra-small few layers MoS_2 nanosheets could grow in-situ inside the semi-concaves HCNB, to obtain the $MoS_2@HCNB$. Contributed by the synergistic effect between HCNB and MoS_2 nanosheets, the MoS_2 nanosheets grown inside the HCNB can form a continuous conductive carbon-MoS_2-carbon network channel with the upper and lower carbon shells inside the carbon nano bowls, which can greatly increase the electrode conductivity of the materials, and HCNB with hierarchical porosity and ultrathin carbon shells promotes electrolyte penetration and provides a conductive shell for excellent charge transfer. However, during the experiment, the internal volume of HCNB is small, which is easy to cause supersaturation impregnation, resulting in the residual MoS_2 on its outer surface rather than achieving perfect carbon-coated MoS_2 structure. Therefore, we choose the best sample in the experiments for further research. Calculated from the TGA results, the MoS_2 content in $MoS_2@HCNB$ accounts for about 14% by weight (Figure S2a).

ii) The **HCNB@MoS$_2$** was synthesized by the solvothermal method using $(NH_4)_2MoS_4$ as both Mo and S sources, the synthesis procedure is shown in **Scheme 1(II)**. Specifically, HCNB was ultrasonically dispersed in ethanol solutions with different concentrations of $(NH_4)_2MoS_4$, and then prepared by the solvothermal method to obtain HCNB@MoS$_2$ with different amount of MoS_2 flakes wrapping on the surface of HCNB. For comparison, we synthesized different amount of MoS_2 wrapped on the surface of HCNB, the three samples were labelled as HCNB@MoS$_2$-1, HCNB@MoS$_2$-2 and HCNB@MoS$_2$-3, containing about 30%, 40% and 60% of MoS_2 by weight according to the TGA results (**Figure S2a and S2b**).

The morphology of the as-prepared HCNB, MoS_2@HCNB and HCNB@MoS_2 samples, was investigated by Scanning Electron Microscope (SEM). **Figure 1a** and **1b** illustrate the surfaces of the HCNB and MoS_2@HCNB, respectively. Both the HCNB and the MoS_2@HCNB, with the average diameters around 200 nm (± 10 nm), have uniform semi-concaved structures with smooth surfaces. The inset of **Figure 1a** shows the fracture surface of HCNB, confirming the hollow structure of the carbon nano bowls. The unnoticeable change of the diameter of the MoS_2@HCNB according to the SEM images (**Figure 1a and Figure 1b**), indicates that the $(NH_4)_2MoS_4$ was perfectly impregnated into the hollow interior of the HCNB by the incipient wetness method and no residue remained on the surface of the HCNB.

The structures and the shell thickness are further characterized by the Transmission Electron Microscopy (TEM, **Figure 1c**) and High Resolution TEM (HRTEM, **Figure 1d**). The thickness of the carbon wall of the shell is about 8 nm, the 2D MoS_2 nanosheets distributed uniformly inside the HCNB. The low thickness, good wettability of the carbon shell and the uniform distribution of MoS_2, are very beneficial to the ions and electron transport for supercapacitor devices. As the carbon walls are very thin, half of the hollow carbon sphere collapsed when removing the silica template. The upper hemisphere continuously sags into the interior, causing the hollow volume inside the carbon nano bowl to be continuously compressed. Finally, a sealing structure similar to the parallel stacking of the two layers of curved carbon nanosheets was formed (**Scheme 1**, **Figure 1a**). The distance between the upper and lower carbon shells is estimated to be around 5-8 nm (**Figure 1f**). This dimension falls in the range of the effective size for the ionic storage of supercapacitor devices, thus can partially contribute to the ionic storage capability.

The unique geometry, morphology and the gap between the two carbon walls, provide an ideal condition under which the ultra-small 2D MoS_2 nanosheets could be formed inside the HCNB. The 2D MoS_2 nanosheets could help to connect the upper and lower carbon layers, forming a network structure with conductive hotpots and channels, which also contribute to the improvement of electrochemical performances. This can be verified by the TEM (**Figure 1c**) clearly, the ultra-small 2D MoS_2 nanosheets with the lateral sizes of 3-5 nm are uniformly dispersed inside the HCNB (indicated by the yellow arrow). The obtained ultra-small size 2D MoS_2 nano crystals and encapsulated structures, indicate that HCNB could provide space-confined nanoreactors to limit the kinetic growth of few-layers ultra-small 2D MoS_2 nanosheets.

The HRTEM characterizations (**Figure 1d**, **1e and 1f**) directly show that the 2D MoS_2 nanosheets grown inside the HCNB have few-layer structures, consisting of one layer, two layers or three layers of MoS_2. The 2D MoS_2 nanosheets exhibit substantial exposed edges which would be electrochemically active sites[30]. The interlayer spacing of the (002) calculated by the Bragg's law is 0.67 nm, larger than that of the bulk MoS_2 (0.62 nm). This is probably due to the chemical intercalation of ammonia produced by the thermal decomposition of $(NH_4)_2MoS_4$[31]. The selected-area electron diffraction (SAED) pattern of the MoS_2@HCNB is shown in **Figure 1e**. The obtained Debye-Scherrer ring patterns of (002), (100), (103) and (110) planes confirmed the crystalline structures of the MoS_2 nanosheets. Combining the density of HCNB and MoS_2@HCNB, and the proportion of MoS_2 in MoS_2@HCNB (from TGA results), it shows that most of MoS_2 is inside HCNB, and very few are outside. Because TGA can indicate that MoS_2 in the material is about 14% of the weight of carbon. The density increases by about 10% (calculated from the **Table S1**). Therefore, it can be said that a very small amount of MoS_2 is on the outer surface of the HCNB, and most of it is wrapped inside. The SEM picture (**Figure 1b**)

reveals that the outer surface of MoS$_2$@HCNB is relatively smooth, which is similar to the pure HCNB sample without MoS$_2$. In addition, the EDX elemental mappings (**Figure 1g-1k**) reveal that there are C, N, O, Mo and S elements in MoS$_2$@HCNB structure. The C, N and O elements are dispersed in the carbon shell, but Mo and S elements are concentrated in the interior of the HCNB framework. This further confirms that MoS$_2$ nanosheets have been grown inside the cavity of HCNB.

The possible mechanism of ultra-small 2D MoS$_2$ nanosheets space confined growth inside HCNB is discussed. The ammonium thiomolybdate solution was adsorbed into the HCNB nanoreactor by vacuum incipient wetness method. A large number of nitrogen-containing and oxygen-containing functional groups within HCNB serve as nucleation sites and deposition sites for coupling Mo precursors, which is beneficial to uniformly disperse the Mo precursor and formation of few-layered MoS$_2$ nanosheets within the HCNB. Subsequently, the MoS$_2$ nanosheets were in situ growth within the HCNB by the following reactions during annealing process: $(NH_4)_2MoS_4 \rightarrow MoS_2 + 2NH_3 + H_2S + 1/8S_8$.[32] At this stage, HCNB as a nanoreactor space confined growth of MoS$_2$ to form ultra-small few-layered nanosheets.

In parallel, the HCNB@MoS$_2$ sample of the similar dimension (diameter 230 ± 20 nm) and same geometry was synthesized and characterized. According to the SEM images in **Figure 2a-2c**, the MoS$_2$ nano flakes are uniformly attached on the surface of the HCNB with different sizes and density. The amount of the MoS$_2$ can be easily controlled by the content of $(NH_4)_2MoS_4$ during the synthesis process. Apparently, at a low $(NH_4)_2MoS_4$ concentration (6 mg/mL), the MoS$_2$ nano flakes are smaller in size (about 20 nm, **Figure 2a**) and uniformly covered the surface of the HCNB. As the content of $(NH_4)_2MoS_4$ increases to 12 mg/mL, the size of the MoS$_2$ nano flakes become significantly larger (about 50-60 nm). An array of interconnected

curly flakes with exposed edges could be found covering the surface of the HCNB (**Figure 2b**). For a high concentration of $(NH_4)_2MoS_4$ (18 mg/mL), it was found that the dense vertically orientated MoS_2 nano flakes (diameter is about 80 nm) were grown and almost completely covered the outer surface of HCNB (**Figure 2c**). The high density and large thickness of the MoS_2 layers, could significantly reduce the conductivity of the composite and degraded the electrochemical properties of the material. According to the TEM images (**Figure 2d** and **Figure S1**), the 2D MoS_2 nano flakes have anchored to the HCNB firmly, same as one can expect strong attachment from the crystal growth steps and mechanism.

The crystallinity of the composites is analyzed by XRD patterns, as shown in **Figure 3a**. The five sharp diffraction peaks at 13.9°, 33.1°, 39.5°, 48.9° and 58.7°, indexed to the (002), (101), (103), (105), (110) planes of 2H phase MoS_2 (JCPDS card No. 371492), implying the high crystallinity of MoS_2 with no byproducts in the MoS_2@HCNB[33]. Compared to the HCNB@MoS_2 (2θ=14.1°), the (002) plane diffraction peak of the MoS_2@HCNB is slightly shifted to 2θ=13.9°. The interplanar spacing of the MoS_2@HCNB calculated by the Bragg's law is 0.66 nm, larger than that of HCNB@MoS_2 (0.64 nm). The increased interplanar spacing provides more space for the inlet and outlet of the ions in the electrolyte, leading to high capability and faster charging and discharging processes[34]. Simultaneously, the (002) peak intensity of MoS_2@HCNB is significantly lower than that of HCNB@MoS_2, indicating that the porous and the unique geometry of HCNB limits the growth of MoS_2. The few layer MoS_2 grew in the (002) direction towards the ultra-small MoS_2 nanosheets inside the hollow carbon to form the MoS_2@HCNB.

In addition, there is a small bump peak around 2θ=20~35° indexed to the (002) crystal orientation of graphitic carbon in the HCNB, which indicates that MoS_2 does not change HCNB

structure either when growing on the outer surface or inside the cavities of the HCNB. The synthesized nano carbon and hybrid materials contain both crystalline and amorphous carbon components. The graphitic carbon structure has been confirmed by G band around 1596 cm^{-1} of the Raman spectra (**Figure 3b**), the in-plane stretching vibrational mode of the sp^2 hybridized carbon atom pair[35]. The characteristic peak around 1372 cm^{-1} is the D band due to the edges, defects and disorder of carbon[36] in the HCNB. The peak intensity ratio (I_D/I_G) provides an approach to evaluate the degree of graphitization of the carbon materials. The I_D/I_G of HCNB, MoS_2@HCNB and HCNB@MoS_2 are close to each other, respectively, indicating that the carbons in all the three samples have a similar degree of graphitization. In addition, there are two peaks at about 379 cm^{-1} and 403 cm^{-1} associated with A_{1g} (out-of-plane symmetric displacements of sulfur atoms along the c-axis) and E_{12g} (the in-plane displacement of Mo and S atoms) of MoS_2 [37].

The Nitrogen sorption isotherms of the obtained carbon and hybrid materials were evaluated by a TriStar 3000 Surface Area and Pore Size Analyzer at 77 K (**Figure 3c**). All the samples, HCNB, MoS_2@HCNB and HCNB@MoS_2 displays type IV isotherm behavior, three typical regions including low pressure ($P/P_0<0.01$), middle pressure ($0.4<P/P_0<0.9$) and high pressure ($P/P_0≈1$) can be clearly distinguished. The surface area of the three materials show big differences (**Figure 3c** and **Table S1**), the MoS_2 carbon hybrid materials have smaller surface areas (734.8 m^2 g^{-1} for the MoS_2@HCNB, 286.1 m^2 g^{-1} for the HCNB@MoS_2) as compared to the pure HCNB (1400 m^2 g^{-1}) or hierarchical porous carbons (1740 m^2 g^{-1})[12]. The reduced surface area of MoS_2@HCNB, is probably due to the ultra-small sized MoS_2 nanosheets grow inside the cavity of HCNB took up some inner space or filled the pores on the surface (consistent with the SEM and TEM analysis results). But for HCNB@MoS_2, the much larger diameter MoS_2

nano flakes wrapped the outer surface of HCNB, severely blocked the pores porosity and led to a significant reduction in surface area (from 1400 m^2 g^{-1} to about 286.1 m^2 g^{-1} only).

The pore size distribution (PSD) was calculated based on the BJH method from the Nitrogen adsorption measurement and plotted in **Figure 3d**. The pore diameters of HCNB, MoS_2@HCNB and HCNB@MoS_2 are ca. 2.25 nm, 2.15 nm and 2.01 nm, respectively. Their pore volumes are 1.17 cm^3 g^{-1}, 0.70 cm^3 g^{-1} and 0.37 cm^3 g^{-1}, showing the same decreasing trend as the surface area changes.

The elemental composition and chemical state of the carbon and MoS_2-carbon hybrid materials were studied by X-ray photoelectron spectroscopy (XPS). The full XPS spectrum confirmed the presence of C, N, O, Mo and S both in the HCNB@MoS_2 and MoS_2@HCNB (**Figure 4a**). The Mo 3d spectra (**Figure 4b**) shows two peaks at 229.1 and 232.3 eV, which is assigned to Mo $3d_{3/2}$ and Mo $3d_{5/2}$, demonstrating Mo^{4+} state in MoS_2. The peak at 235.7 eV is attributed to Mo^{6+} due to partial oxidation by O atom in carbon layers and MoS_2[38]. The S 2p spectra (**Figure 4c**) consists of two peaks at 163.2 and 162.1 eV that are related to S $2p_{3/2}$ and S $2p_{1/2}$ of S^{2-}, which is representing the split spin doublet for the p-orbital of S^{2-}[38]. The atomic ratio of Mo to S is about 1:2, further confirming the synthesis of MoS_2 in the composites. The high resolution XPS spectra of C 1s, O1s and N 1s confirmed the successful doping of N and O in HCNB (**Figure 4d-4e**). However, HCNB has been first heat-treated at 900°C. Then, after incipient wetness impregnation of the MoS_2 precursor, heat treatment is performed only at 400 °C. Therefore, the possibility of C doping into MoS_2 is very small. As seen in **Figure 4f** and **Table S2**, the nitrogen and oxygen contents for MoS_2@HCNB and HCNB@MoS_2 are more than HCNB. This is due to the chemical intercalation of ammonia and oxidation by the thermal decomposition of $(NH_4)_2MoS_4$, which can be beneficial to their wettability and provide partial pseudo-capacitance.

Large specific surface area and proper pore size distributions and elemental doping are critically important and represent a direct correlation with the electrochemical energy storage capability of the supercapacitors, as they are based on the formation of electric double layer by ion electrosorption at the electrode-electrolyte surface. A typical porous carbon material with the specific surface area of 1000 m^2/g, whose double-layer capacitance is about 10 $\mu F/cm^2$, typically lead to the specific capacitance of about 100 F/g[4]. Among the samples synthesized, the HCNB and MoS_2@HCNB, has the larger BET surface area, high pore volume and suitable pore size (2-5 nm) that falls into the electric double cylinder capacitor range[39]. Theoretically, the HCNB and MoS_2@HCNB should have a better electric double layer capacitance than HCNB@MoS_2.

The obtained carbon and hybrid nano materials were used as electrodes of supercapacitor devices, the electrochemical tests were carried out. **Figure 5a** is the Cyclic Voltammetry (CV) curves of HCNB, HCNB@MoS_2 and MoS_2@HCNB electrodes (scanning rate of 5 mV s^{-1}). The CV curves of these samples are quasi-rectangular, indicating the domination of the electric double layer capacitance (EDLC) with minor faradaic pseudocapacitance.

The samples were evaluated at different scanning rates from 5 to 200 mV s^{-1} (**Figure 5b and Figure S3a-S3b and Figure S5a-5c**). Even at the high scanning rate of 200 mV s^{-1}, the deformation of the CV curve of MoS_2@HCNB is still not very significant, which means that the electrode is charged and discharged at a pseudo-constant rate over the complete voltammetric cycle. The CV curve at the faster scan rate has a larger area than the lower scan rate one, but does not indicate a greater charge capacitance at the higher scan rate. Meanwhile, with the scan rate increases, the effective interaction between the ions and the electrode is greatly reduced because of the resistance of MoS_2 and the deviation from rectangularity of the CV becomes obviously. These results prove that the success of the spatially confined growth of ultra-small

MoS$_2$ nanosheets inside the HCNB, is a promising approach towards the synthesis of higher performance supercapacitor materials.

The Galvanostatic Charge-Discharge (GCD) curves of HCNB, HCNB@MoS$_2$ and MoS$_2$@HCNB at 0.2 A g^{-1} in 6M KOH electrolyte are shown in **Figure 5c**. The GCD curve of HCNB shows a typical isosceles triangular shape, indicating the dominant double layer capacitive behavior along with minor pseudocapacitance due to the N and O doping in the carbon materials. The mechanism of MoS$_2$ contribution to the capacity mainly includes three aspects, besides the electric double layer capacity and the pseudocapacitive (contributed by the redox reaction of Mo atoms), the larger spacing of 2D MoS$_2$ layers can accelerate the rapid reversible intercalation of electrolyte ions (H$^+$, K$^+$, NH$_4^+$) between few layers, which can also partially contribute with the embedded pseudocapacitance. The theoretical specific capacity of MoS$_2$ is as high as 1200 F g^{-1} (**detailed information displayed on SI12**). In contrast, the GCD curves of HCNB@MoS$_2$ and MoS$_2$@HCNB were distorted due to the pseudocapacitances from the MoS$_2$ nanosheets. The pseudocapacitance of MoS$_2$ is due to the faradaic charge transfer of Mo during the electrochemical process[16], in which Mo could show several oxidation states from +2 to +6, so it can show a pseudocapacitor similar to RuO$_2$. The gravimetric capacitances (C_g) of the HCNB, HCNB@MoS$_2$ and MoS$_2$@HCNB electrodes are calculated by the equation,

$$C_g = I\Delta t/m\Delta V \qquad (1)$$

where, I is the current density, Δt is the discharge time, m is the weight of the active material, and ΔV is the potential window. Interestingly, though the MoS$_2$@HCNB whose surface area is not the highest, it has the largest closed area of its CV curve (**Figure 5a**) corresponding to a higher specific capacitance (560 F g^{-1}) than HCNB@MoS$_2$ (370 F g^{-1}) and HCNB (272 F g^{-1}, **Figure 5d**).

The volumetric capacitance C_v is calculated from the equation of $C_v = C_g \times \rho$. The volumetric capacitance C_v is another important parameter for supercapacitors, especially when the supercapacitors are applied in miniaturized and portable electronic products. The MoS_2 nanosheets can improve the packing density (ρ) of the electrode materials (also shown in **Table S1**). The packing densities were evaluated by placing 100mg samples into a dry measuring cylinder, then taped hundreds of times **(Figure S6).** Notably, HCNB with semi-concave structure is derived from the collapse of hollow spheres, which makes it can be densely stacked and has an enhanced packing density than other carbon electrode materials. In addition, $MoS_2@HCNB$, which confine the growth of ultra-small MoS_2 nanosheets within the HCNB, did not alter the backbone structure of the HCNB. Therefore, the $MoS_2@HCNB$ is about 10% higher packing density (1.56 g cm^{-3}) than HCNB (1.41 g cm^{-3}). As shown in **Figure 6a**, $MoS_2@HCNB$ electrode has the largest volumetric capacitance of 874 F cm^{-3}. As the volumetric capacitance is more than twice of that of the HCNB (370 F cm^{-3}), the remarkable improvement cannot be only explained by the higher packing density (only about 10% higher). The boosted performance stems from its higher gravimetric capacitance together with enhanced packing density.

The gravimetric capacitances were obtained based on the GCD curves at varied current densities (**Figure S4 and Figure S5d-5f**). The gravimetric capacitance of $MoS_2@HCNB$ is 433 F g^{-1} at high current density (10 A g^{-1}), and the capacitor retention is 77.3% which was obviously higher than HCNB@MoS_2 (only 63.5%). **Figure 6b** and **Table S3** compare the gravimetric capacitance and the volumetric capacitance of the $MoS_2@HCNB$ with other materials previously reported, such as porous carbon[40, 41], carbon nanotubes (CNTs)[42], graphene[43, 44], MXene[45], MoS_2[19, 46, 47], verifying that this new synthetic strategy makes it be possible for $MoS_2@HCNB$ to achieve excellent gravimetric capacitance as well as volumetric

capacitance. The better rate performance is attributed to the space-confined nanoreactors of HCNB and the ultra-small MoS_2 nanosheets with few layers structures.

In order to study the charge transfer kinetics and internal resistance, the electrochemical impedance spectroscopy (EIS) tests were carried out at the frequency from 10^{-1} to 10^5 Hz. The charge transfer resistance (R_{ct}) is 1.2 Ω, 2.2 Ω and 3.7 Ω for HCNB, MoS_2@HCNB and HCNB@MoS_2, estimated from the Nyquist plot (**Figure 6c**) of the three materials. The MoS_2@HCNB with 2D MoS_2 nanosheet grown inside the cavity of HCNB, has better conductivity than HCNB@MoS_2, revealing the excellent interfacial contact between the ultra-small few layer MoS_2 nanosheets and HCNB. The low R_{ct} indicates that the MoS_2@HCNB could promote faster ion diffusion and enhance energy storage for the supercapacitors.

The cycle life of the samples was evaluated and plotted in **Figure 6d**. Both of the HCNB and MoS_2@HCNB electrodes maintained high capacitance retention as high as 96.7% and 94.4% after 5000 cycles, much higher that of HCNB@MoS_2 (78.1%). Furthermore, the morphology of the of HCNB, MoS_2@HCNB and HCNB@MoS_2 electrodes after the cycling tests were observed by SEM, and the results are shown in **Figure S7**. It is clearly shown that the size, shape, and structural integrity of the carbon nano bowl skeleton are unchanged. The excellent cycling stability of MoS_2@HCNB reveals that carbon nano bowls can act as rigid shields, which can effectively alleviate the structural deformation caused by the MoS_2 during the charge-discharge processes.

The MoS_2@HCNB where the ultra-small MoS_2 nanosheets grown inside the cavity of HCNB, exhibits larger gravimetric capacitance (560 F g^{-1}), much higher than that of HCNB@MoS_2 (370 F g^{-1}) or HCNB (272 F g^{-1}). The MoS_2 nanosheets growing inside of HCNB are only a few nanometers (about 3-5 nm), much smaller than MoS_2 nano flakes (20-80 nm) covered on the

18

surface of HCNB. Therefore, the electrolyte ions could easily reach the interlayers reaction sites of MoS_2 and adsorbed on the 2D surfaces to exhibit electrochemical double layer capacitance or to induce faradaic reaction and pseudocapacitance. In addition, the few layer MoS_2 nanosheets growing inside the HCNB are uniformly distributed, thus formed a continuous conductive bridging with the upper and lower carbon shells inside the carbon nano bowls, which can greatly increase the electrode conductivity of the materials. Finally, the high BET surface area, developed hierarchical porous structures and larger pore volumes also contribute to the improvement of specific capacitance performance. The performances achieved represent one of the best results on the MoS_2 or carbon based supercapacitor devices (**Figure 6b**). It provides a new strategy both for the space confined growth of 2D layered materials, as well as the development of high performance supercapacitor materials.

CONCLUSIONS

In conclusion, ultra-small MoS_2 nanosheets with few layer structure were space-confined grown inside of N-doped Hollow Carbon Nano Bowls (HCNB) by a facile method. The semi-concave structured HCNB has a high specific surface area, hierarchical porosity and ultrathin carbon shells, which can provide electrochemical double layer capacitance. MoS_2 nanosheets with few layers of structure and ultra-small diameter allowed the rapid reversible intercalation of electrolyte ions between layers, which can contribute a part of the embedded pseudocapacitance. In addition, contributed by the synergistic effect between HCNB and MoS_2 nanosheets, the MoS_2 nanosheets grown inside the HCNB can form a continuous conductive carbon-MoS_2-carbon network channel with the upper and lower carbon shells inside the carbon nano bowls, which can greatly increase the electrode conductivity of the materials, and HCNB with hierarchical porosity and ultrathin carbon shells promotes electrolyte penetration and provides a conductive shell for

excellent charge transfer. Furthermore, the HCNB with a unique semi-concave geometry tightly enfolds the ultra-small size, few layer MoS_2 nanosheets, which can protect the structural stability while enhancing the volumetric capacitance of the hybrid MoS_2@HCNBs. Consider all of these advantages, MoS_2@HCNB as the electrode material applied in supercapacitors, can simultaneously obtain excellent gravimetric capacitance (560 F g^{-1}) and volumetric capacitance (874 F cm^{-3}), and enhanced cycling performance (94.4% capacitance retention after 5000 cycles) than HCNB@MoS_2 where the MoS_2 nano flakes grew on the outer surface of HCNB. The present work paved the way to the further development of space-confined reaction inside HCNB, which can also be easily extended to the construction of other 2D nanostructures (such as metal sulfide/oxide) for other applications, such as catalysis, biomedicine, gas storage and drug delivery.

Experimental Section

Synthesis of hollow carbon nano bowls with semi-concaves structure (HCNB)[48]: HCNB was prepared by a facile method using SiO_2 as a hard template, tetraethyl orthosilicate as pore-forming agent. Typically, 0.5 g of SiO_2 was uniformly dispersed in a premixed solution of ethanol and deionized water (ethanol: water = 3:7), then resorcinol, formaldehyde and ethylenediamine were sequentially added to the above solution under stirring at 35 °C. After 10 minutes, a certain amount of TEOS was added dropwise with vigorous stirring, and the reaction was continued for 24 hours. After centrifugation and drying, the sample was carbonized at 900 °C for 3 h under N_2. The HCNB with a novel semi-concave geometry was obtained by removing the silica with a 10% hydrofluoric acid (HF) solution.

Synthesis of MoS_2@HCNB: MoS_2@HCNB was prepared by vacuum incipient wetness impregnation. The obtained HCNB was placed in a closed glass vessel and degassed for 30

minutes to obtain a vacuum state. Under the vacuum, the ammonium thiomolybdate dissolved in ethanol is added dropwise until incipient wetness and then dried at 80 °C overnight. Finally, heat treatment was carried out for 3h at 350 °C under N_2 atmosphere to obtain MoS$_2$@HCNB.

Synthesis of HCNB@MoS$_2$: HCNB@MoS$_2$ was produced by a simple solvothermal process. A certain amount of ammonium thiomolybdate was dissolved in 20 ml of ethanol, after stirring for 30 min, 25 mg of HCNB was added and mixed by stirring for 2 hours. The solution was then transferred into a 30 mL Teflon autoclave and kept at 200 °C for 15 hours. After collection, the sample was calcined for 3 hours at 350 °C under N_2 atmosphere to obtain the HCNB@MoS$_2$.

Characterizations: The morphologies and structures of the HCNB, MoS$_2$@HCNB and HCNB@MoS$_2$ were conducted by scanning electron microscopy (SEM, FEI Sirion200) and transmission electron microscopy (TEM, EM-2100F JEOL). X-ray diffractometer (XRD D8 ADVANCE Da Vinci with Cu Kα radiation), X-ray photoelectron spectroscope (XPS Kratos AXIS Ultra DLD) and Raman spectrometer (Horiba JobinYvon HR 800 Raman spectrometer) were used to characterize the chemical compositions of samples. Thermo-gravimetric analyses (TGA) were performed by a thermo-gravimetric analyzer (NETZSCH STA 449F3) under atmosphere. The specific surface area and pore structure were tested at 77 K on a TriStar 3000 Surface Area and Pore Size Analyzer. The packing density of the materials was determined by the method reported in the literature [56].

Electrochemical characterizations: The electrode was prepared by coating mixed slurry of active material, acetylene black and PVDF (polytetrafluoroethylene) with the weight ratio of 8:1:1 on the nickel foam as the current collector (1 × 1 cm), and then dried at 100°C overnight. The mass of active materials was kept at about 2.0 mg cm^{-2}, and the electrode thickness was about 100 μm (**Figure S8**). The Hg/HgO electrode and a piece of Pt were used as reference and

counter electrode, respectively. The electrochemical measurements were carried out by a CHI 660D potentiostat (CHI instrument, Shanghai, China) using 6 M KOH as the electrolyte. The voltage for CV and GCD varied from 0 V to 1 V. The scanning rates of the CV were from 5 to 200 mV s^{-1} and the current densities of GCD were from 0.2 to 10.0 A g^{-1}. The EIS spectra were obtained in a frequency range from 10^{-1} to 10^5 Hz.

ASSOCIATED CONTENT

Supporting Information

TEM images of HCNB@MoS$_2$-1 and HCNB@MoS$_2$-3 (Figure S1), TGA curves of HCNB, MoS$_2$@HCNB and HCNB@MoS$_2$ (Figure S2), CV curves at the various scanning rates for HCNB and HCNB@MoS$_2$ (Figure S3), GCD curves at the various scanning rates for HCNB, MoS$_2$@HCNB and HCNB@MoS$_2$ (Figure S4), CV and GCD curves at the various scanning rates for HCNB@MoS$_2$ samples with different amount of MoS$_2$ wrapped on the surface of HCNB (Figure S5). A photograph of 100 mg of HCNB, MoS$_2$@HCNB and HCNB@MoS$_2$ tapped in quartz tubes (Figure S6). SEM characterizations of HCNB, MoS$_2$@HCNB and HCNB@MoS$_2$ electrodes after 5000 discharge/charge cycles at 5.0 A g^{-1} (**Figure S7**), and SEM images of the electrode thickness for HCNB, MoS$_2$@HCNB and HCNB@MoS$_2$ electrodes (Figure S8). Textural parameters and compacting densities of HCNB, MoS$_2$@HCNB and HCNB@MoS$_2$ (Table S1), Elemental composition of HCNB, MoS$_2$@HCNB and HCNB@MoS$_2$ by XPS (Table S2), Comparison of the as-prepared electrode materials with previously reported related materials(Table S3) and Estimation of the theoretical specific capacity of MoS$_2$.

The following files are available free of charge.

Supporting Information (file type, PDF)

AUTHOR INFORMATION

Corresponding Authors

Binyuan Zhao*, Lifeng Zhang*, Weiping Wu*

E-mail: byzhao@sjtu.edu.cn, zhanglifeng@sust.edu.cn, Weiping.Wu@city.ac.uk

Author Contributions

The manuscript was written through contributions of all authors. All authors have given approval to the final version of the manuscript.

Notes

The authors declare no competing financial interest.

REFERENCES

(1) Simon, P.; Gogotsi, Y.; Dunn, B. Where Do Batteries End and Supercapacitors Begin? *Science* **2014**, 343, 1210−1211.

(2) Conway, B. E. Transition From "Supercapacitor" to "Battery" Behavior in Electrochemical Energy Storage. *J. Electrochem. Soc.* **1991**, 138, 1539−1548.

(3) Conway, B. E.; Birss, V.; Wojtowicz, J. The Role and Utilization of Pseudocapacitance for Energy Storage by Supercapacitors. *J. Power Sources* **1997**, 66, 1−14.

(4) Yan, J.; Wang, Q.; Wei, T.; Fan, Z. J. Recent Advances in Design and Fabrication of Electrochemical Supercapacitors with High Energy Densities. *Adv. Energy Mater.* **2014**, 4, 1300816.

(5) Novoselov, K. S.; Geim, A. K.; Morozov, S. V.; Jiang, D.; Zhang, Y.; Dubonos, S. V.; Grigorieva, I. V.; Firsov, A. A. Electric Field Effect in Atomically Thin Carbon Films. *Science* **2004**, 306, 666−669.

(6) Torrisi, F.; Hasan, T.; Wu, W. P.; Sun, Z. P.; Lombardo, A.; Kulmala, T. S.; Hsieh, G. W.; Jung, S. J.; Bonaccorso, F.; Paul, P. J.; Chu, D. P.; Ferrari, A. C. Inkjet-Printed Graphene Electronics. *ACS Nano* **2012**, 6, 2992−3006.

(7) Gourmelon, E.; Lignier, O.; Hadouda, H.; Couturier, G.; Bernede, J. C.; Tedd, J.; Pouzet, J.; Salardenne, J. MS_2 (M=W, Mo) Photosensitive Thin Films for Solar Cells. *Sol. Energy Mater. Sol. Cells* **1997**, 46, 115−121.

(8) Yoo, E.; Kim, J.; Hosono, E.; Zhou, H.; Kudo, T.; Honma, I. Large Reversible Li Storage of Graphene Nanosheet Families for Use in Rechargeable Lithium Ion Batteries. *Nano Lett.* **2008**, 8, 2277–2282.

(9) Chen, R. J.; Zhao, T.; Wu, W. P.; Wu, F.; Li, L.; Qian, J.; Xu, R.; Wu, H. M.; Albishri, H. M.; Al-Bogami, A. S.; Abd El-Hady, D.; Lu, J.; Amine, K. Free-Standing Hierarchically Sandwich-Type Tungsten Disulfide Nanotubes/Graphene Anode for Lithium-Ion Batteries. *Nano Lett.* **2014**, 14, 5899–5904.

(10) Ren, W. N.; Zhang, H. F.; Guan, C.; Cheng, C. W. Ultrathin MoS_2 Nanosheets@Metal Organic Framework-Derived N-Doped Carbon Nanowall Arrays as Sodium Ion Battery Anode with Superior Cycling Life and Rate Capability. *Adv. Funct. Mater.* **2017**, 27, 1702116.

(11) Liu, F. H.; Zhao, B. Y.; Wu, W. P.; Yang, H. Y.; Ning, Y. S.; Lai, Y. J.; Bradley, R. Low Cost, Robust, Environmentally Friendly Geopolymer-Mesoporous Carbon Composites for Efficient Solar Powered Steam Generation. *Adv. Funct. Mater.* **2018**, 28, 1803266.

(12) Liu, F. H.; Wang, L. J.; Bradley, R.; Zhao, B. Y.; Wu, W. P. Highly Efficient Solar Seawater Desalination with Environmentally Friendly Hierarchical Porous Carbons Derived from Halogen-Containing Polymers. *RSC Adv.* **2019**, 9, 29414–29423.

(13) Liu, F. H.; Lai, Y. J.; Zhao, B. Y.; Bradley, R.; Wu, W. P. Photothermal Materials for Efficient Solar Powered Steam Generation. *Front. Chem. Sci. Eng.* **2019**, 13, 636–653.

(14) Liu, F. H.; Wang, L. J.; Bradley, R.; Zhao, B. Y.; Wu, W. P. Graphene-Carbon Composites for Solar and Low-Voltage Powered Efficient Interfacial Evaporation. *Adv. Sustain. Syst.* **2020**, 4, 1900122.
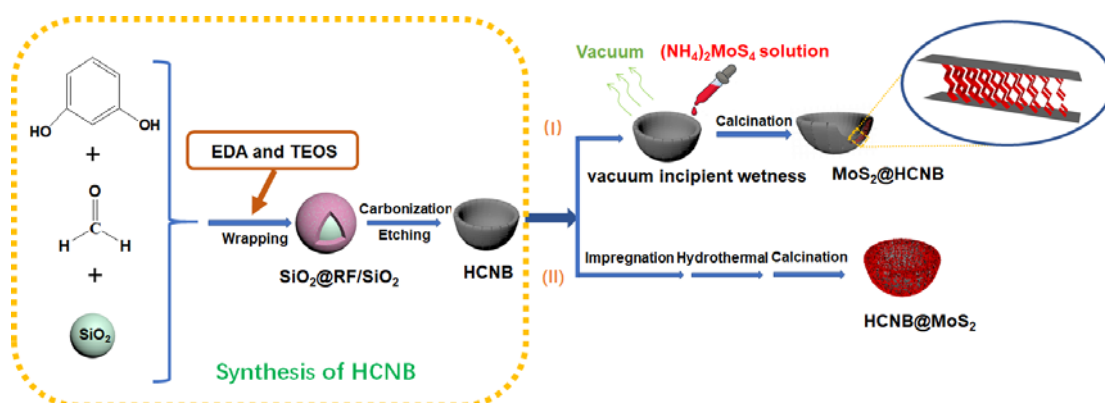
(15) Liu, C. G.; Yu, Z. N.; Neff, D.; Zhamu, A.; Jang, B. Z. Graphene-Based Supercapacitor with an Ultrahigh Energy Density. *Nano Lett.* **2010**, 10, 4863−4868.

(16) Soon, J. M.; Loh, K. P. Electrochemical Double-Layer Capacitance of MoS_2 Nanowall Films. *Solid-State Lett.* **2007**, 10, A250−A254.

(17) Li, S. Z.; Zang, W. J.; Liu, X. M.; Pennycook, S. J.; Kou, Z. K.; Yang, C. H.; Guan, C.; Wang, J. Heterojunction Engineering of $MoSe_2$/MoS_2 with Electronic Modulation Towards Synergetic Hydrogen Evolution Reaction and Supercapacitance Performance. *Chem. Eng. J.* **2019**, 359, 1419−1426.

(18) Radisavljevic, B.; Radenovic, A.; Brivio, J.; Giacometti, V.; Kis, A. Single-Layer MoS_2 Transistors. *Nat. Nanotechnol.* **2011**, 6, 147−150.

(19) Acerce, M.; Voiry, D.; Chhowalla, M. Metallic 1T Phase MoS_2 Nanosheets as Supercapacitor Electrode Materials. *Nat. Nanotechnol.* **2015**, 10, 313−318.

(20) Zhu, Y. W.; Murali, S.; Stoller, M. D.; Ganesh, K. J.; Cai, W. W.; Ferreira, P. J.; Pirkle, A.; Wallace, R. M.; Cychosz, K. A.; Thommes, M.; Su, D.; Stach, E. A.; Ruoff, R. S. Carbon-Based Supercapacitors Produced by Activation of Graphene. *Science* **2011**, 332, 1537−1541.

(21) Tang, H. J.; Wang, J. Y.; Yin, H. J.; Zhao, H. J.; Wang, D.; Tang, Z. Y. Growth of Polypyrrole Ultrathin Films on MoS_2 Monolayers as High-Performance Supercapacitor Electrodes. *Adv. Mater.* **2015**, 27, 1117−1123.

(22) Ji, H. M.; Liu, C.; Wang, T.; Chen, J.; Mao, Z. N.; Zhao, J.; Hou, W. H.; Yang, G. Porous Hybrid Composites of Few-Layer MoS_2 Nanosheets Embedded in a Carbon Matrix with an Excellent Supercapacitor Electrode Performance. *Small* **2015**, 11, 6480−6490.

(23) Luo, Y. F.; Zhang, Y.; Zhao, Y.; Fang, X.; Ren, J.; Weng, W.; Jiang, Y. S.; Sun, H.; Wang, B. J.; Cheng, X. L.; Peng, H. S. Aligned Carbon Nanotube/Molybdenum Disulfide Hybrids for Effective Fibrous Supercapacitors and Lithium Ion Batteries. *J. Mater. Chem. A* **2015**, 3, 17553–17557.

(24) Pomerantseva, E.; Gogotsi, Y. Two-Dimensional Heterostructures for Energy Storage. *Nat. Energy* **2017**, 2, 17089.

(25) Ju, J. G.; Zhang, L. T.; Shi, H. S.; Li, Z. J.; Kang, W. M.; Cheng, B. W. Three-Dimensional Porous Carbon Nanofiber Loading MoS_2 Nanoflake-Flowerballs as a High-Performance Anode Material for Li-Ion Capacitor. *Appl. Surf. Sci.* **2019**, 484, 392–402.

(26) Li, S. J.; Pasc, A.; Fierro, V.; Celzard, A. Hollow Carbon Spheres, Synthesis and Applications - a Review. *J. Mater. Chem. A* **2016**, 4, 12686–12713.

(27) Yu, M. H.; Qiu, W. T.; Wang, F. X.; Zhai, T.; Fang, P. P.; Lu, X. H.; Tong, Y. X. Three Dimensional Architectures: Design, Assembly and Application in Electrochemical Capacitors. *J. Mater. Chem. A* **2015**, 3, 15792–15823.

(28) Lu, X. H.; Liu, T. Y.; Zhai, T.; Wang, G. M.; Yu, M. H.; Xie, S. L.; Ling, Y. C.; Liang, C. L.; Tong, Y.; Li, Y. Improving the Cycling Stability of Metal- Nitride Supercapacitor Electrodes with a Thin Carbon Shell. *Adv. Energy Mater.* **2014**, 4, 1300994.

(29) Lei, J. Y.; Jiang, Z. Q.; Lu, X. F.; Nie, G. D.; Wang, C. Synthesis of Few-Layer MoS_2 Nanosheets-Wrapped Polyaniline Hierarchical Nanostructures for Enhanced Electrochemical Capacitance Performance. *Electrochim. Acta* **2015**, 176, 149–155.

(30) Wang, Z.; Chen, T.; Chen, W. X.; Chang, K.; Ma, L.; Huang, G. C.; Chen, D. Y.; Lee, J. Y. CTAB-Assisted Synthesis of Single-Layer MoS_2-Graphene Composites as Anode Materials of Li-ion Batteries. *J. Mater. Chem. A* **2013**, 1, 2202–2210.

(31) Zhang, X.; Zhao, R. F.; Wu, Q. H.; Li, W. L.; Shen, C.; Ni, L. B.; Yan, H.; Diao, G. W.; Chen, M. Petal-Like MoS_2 Nanosheets Space-Confined in Hollow Mesoporous Carbon Spheres for Enhanced Lithium Storage Performance. *ACS Nano* **2017**, 11, 8429–8436.

(32) Afanasiev, P.; Bezverkhyy, I. Ternary Transition Metals Sulfides in Hydrotreating Catalysis. *Appl. Catal., A* **2007**, 322, 129–141.

(33) Fan, X. B.; Xu, P. T.; Zhou, D. K.; Sun, Y. F.; Li, Y. G. C.; Nguyen, M. A. T.; Terrones, M.; Mallouk, T. E. Fast and Efficient Preparation of Exfoliated 2H MoS_2 Nanosheets by Sonication-Assisted Lithium Intercalation and Infrared Laser-Induced 1T to 2H Phase Reversion. *Nano Lett.* **2015**, 15, 5956–5960.

(34) Stephenson, T.; Li, Z.; Olsen, B.; Mitlin, D. Lithium Ion Battery Applications of Molybdenum Disulfide (MoS_2) Nanocomposites. *Energy Environ. Sci.* **2014**, 7, 209–231.

(35) Ferrari, A. C.; Meyer, J. C.; Scardaci, V.; Casiraghi, C.; Lazzeri, M.; Mauri, F.; Piscanec, S.; Jiang, D.; Novoselov, K. S.; Roth, S.; Geim, A. K. Raman Spectrum of Graphene and Graphene Layers. *Phys. Rev. Lett.* **2006**, 97, 187401.

(36) Ferrari, A. C.; Robertson, J. Interpretation of Raman Spectra of Disordered and Amorphous Carbon. *Phys. Rev. B* **2000**, 61, 14095–14107.

(37) Frey, G. L.; Tenne, R.; Matthews, M. J.; Dresselhaus, M. S.; Dresselhaus, G. Raman and Resonance Raman Investigation of MoS_2 Nanoparticles. *Phys. Rev. B* **1999**, 60, 2883–2892.

(38) Ganta, D.; Sinha, S.; Haasch, R. T. 2-D Material Molybdenum Disulfide Analyzed by XPS. *Surf. Sci. Spectra* **2014**, 21, 19–27.

(39) Kondrat, S.; Perez, C. R.; Presser, V.; Gogotsi, Y.; Kornyshev, A. A. Effect of Pore Size and Its Dispersity on the Energy Storage in Nanoporous Supercapacitors. *Energy Environ. Sci.* **2012**, 5, 6474–6479.

(40) Guo, D. C.; Mi, J.; Hao, G. P.; Dong, W.; Xiong, G.; Li, W. C.; Lu, A. H. Ionic Liquid $C_{16}mimBF_4$ Assisted Synthesis of Poly(Benzoxazine-Co-Resol)-Based Hierarchically Porous Carbons with Superior Performance in Supercapacitors. *Energy Environ. Sci.* **2013**, 6, 652–659.

(41) Yu, X. L.; Wang, J. G.; Huang, Z. H.; Shen, W. C.; Kang, F. Y. Ordered Mesoporous Carbon Nanospheres as Electrode Materials for High-Performance Supercapacitors. *Electrochem. Commun.* **2013**, 36, 66–70.

(42) Cai, Z. J.; Zhang, Q.; Song, X. Y. Improved Electrochemical Performance of Polyindole/Carbon Nanotubes Composite as Electrode Material for Supercapacitors. *Electron Mater. Lett.* **2016**, 12, 830–840.

(43) Pham, V. H.; Dickerson, J. H. Reduced Graphene Oxide Hydrogels Deposited in Nickel Foam for Supercapacitor Applications: Toward High Volumetric Capacitance. *J. Phys. Chem. C* **2016**, 120, 5353–5360.

(44) Yu, P. P.; Zhao, X.; Huang, Z. L.; Li, Y. Z.; Zhang, Q. H. Free-Standing Three-Dimensional Graphene and Polyaniline Nanowire Arrays Hybrid Foams for High-Performance Flexible and Lightweight Supercapacitors. *J. Mater. Chem. A* **2014**, 2, 14413–14420.

(45) Ghidiu, M.; Lukatskaya, M. R.; Zhao, M. Q.; Gogotsi, Y.; Barsoum, M. W. Conductive Two-Dimensional Titanium Carbide 'Clay' with High Volumetric Capacitance. *Nature* **2014**, 516, 78−81.

(46) Thakur, A. K.; Majumder, M.; Choudhary, R. B.; Singh, S. B. MoS$_2$ Flakes Integrated with Boron and Nitrogen-Doped Carbon: Striking Gravimetric and Volumetric Capacitive Performance for Supercapacitor Applications. *J. Power Sources* **2018**, 402, 163−173.

(47) Majumder, M.; Choudhary, R. B.; Koiry, S. P.; Thakur, A. K.; Kumar, U. Gravimetric and Volumetric Capacitive Performance of Polyindole/Carbon Black/MoS$_2$ Hybrid Electrode Material for Supercapacitor Applications. *Electrochim. Acta* **2017**, 248, 98−111.

(48) Wang, L.; Liu, F.; Ning, Y.; Bradley, R.; Yang, C.; Yong, K.-T.; Zhao, B.; Wu, W. Biocompatible Mesoporous Hollow Carbon Nanocapsules for High Performance Supercapacitors. *Sci. Rep.* **2020**, 10, 4306−4306.

Scheme 1. Schematic synthesis processes of the hierarchical MoS$_2$-Carbon Nano Spherical Bowls (HCNB) hybrid materials, (I) MoS$_2$@HCNB and (II) HCNB@MoS$_2$.
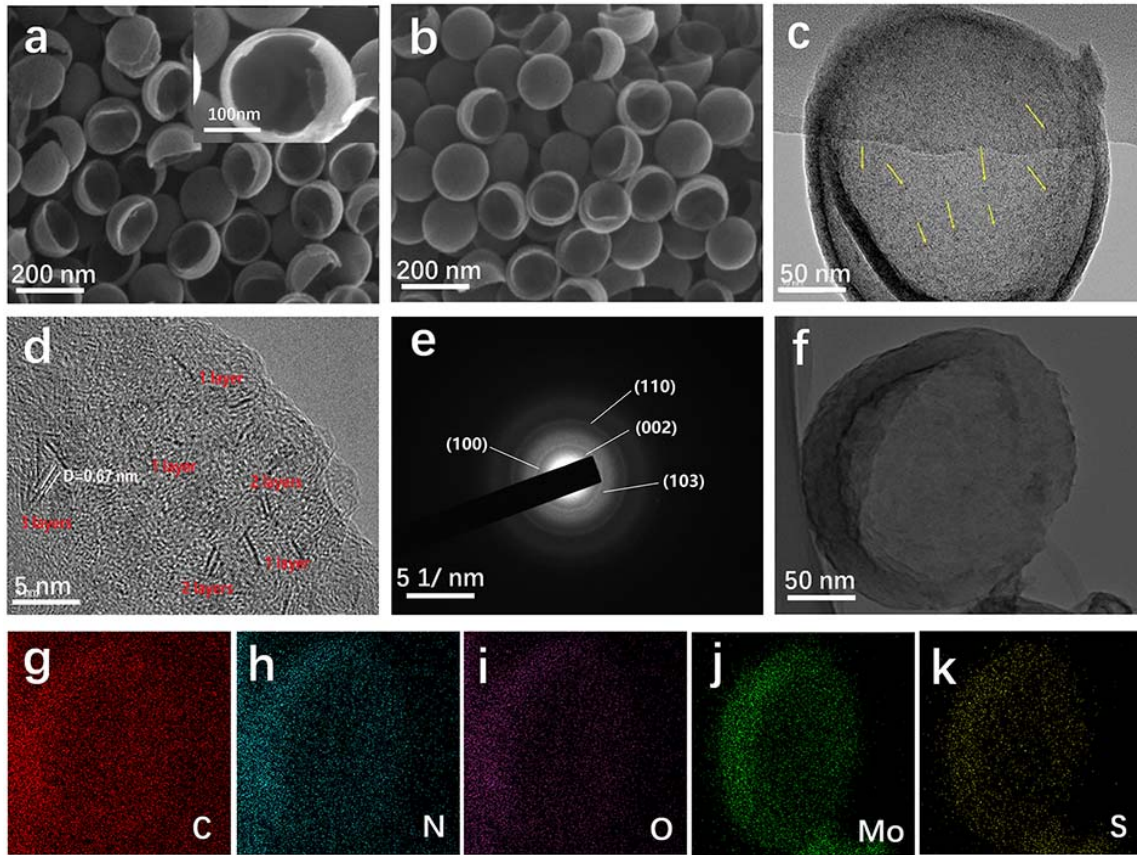
Fig. 1. SEM images of (a) HCNB (the inset is the fracture surface of an HCNB) and (b) MoS$_2$@HCNB, (c) TEM image of MoS$_2$@HCNB. (d) HRTEM image of MoS$_2$@HCNB, (e) Selected-area electron diffraction (SAED) pattern of MoS$_2$@HCNB, (f) STEM image, (g-k) the corresponding Energy Dispersive X-Ray (EDX) elemental mappings of C, N, O, Mo and S in a single MoS$_2$@HCNB.
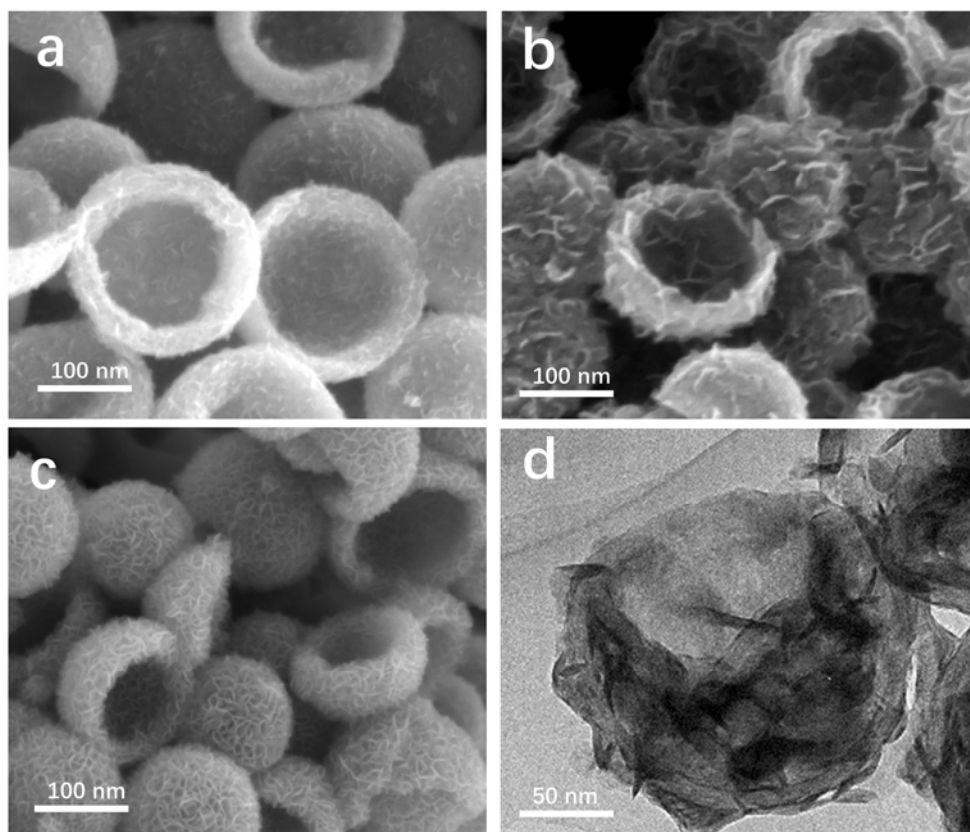
Fig. 2. SEM images of the as-prepared HCNB@MoS$_2$ samples with different amount of MoS$_2$ wrapped on the surface of HCNB, (a) HCNB@MoS$_2$-1, (a) HCNB@MoS$_2$-2 and (c) HCNB@MoS$_2$-3, (d) TEM image of HCNB@MoS$_2$-2.
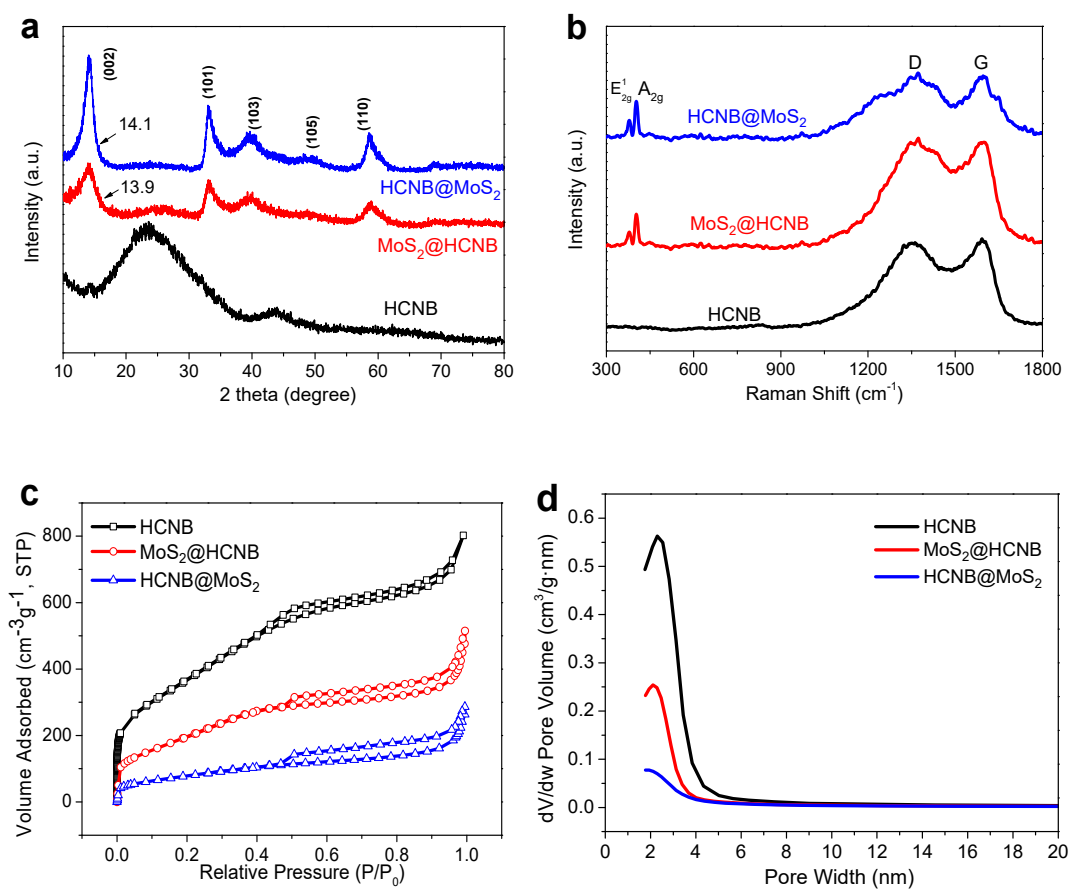
Fig. 3. (a) XRD patterns and (b) Raman spectrum of HCNB, MoS_2@HCNB and HCNB@MoS_2. (c) Nitrogen adsorption–desorption isotherms of the HCNB, MoS_2@HCNB and HCNB@MoS_2. (d) Pore size distributions of the three samples.
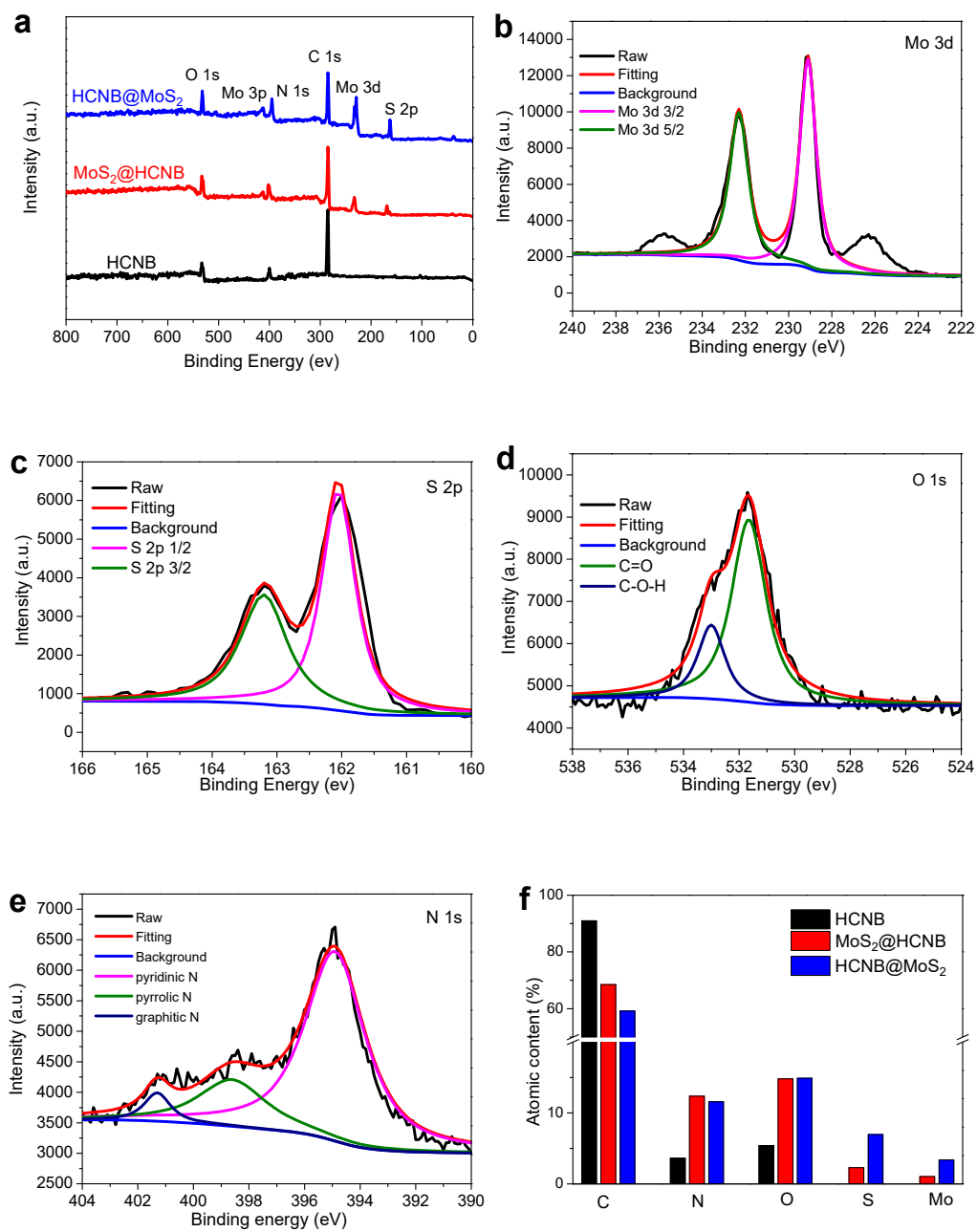
Fig. 4. (a) XPS survey spectrum, and high-resolution spectra of (b) Mo 3d, (c) S 2p, (d) O 1s and (e) N 1s of MoS₂@HCNB, and (f) atomic content in the samples.
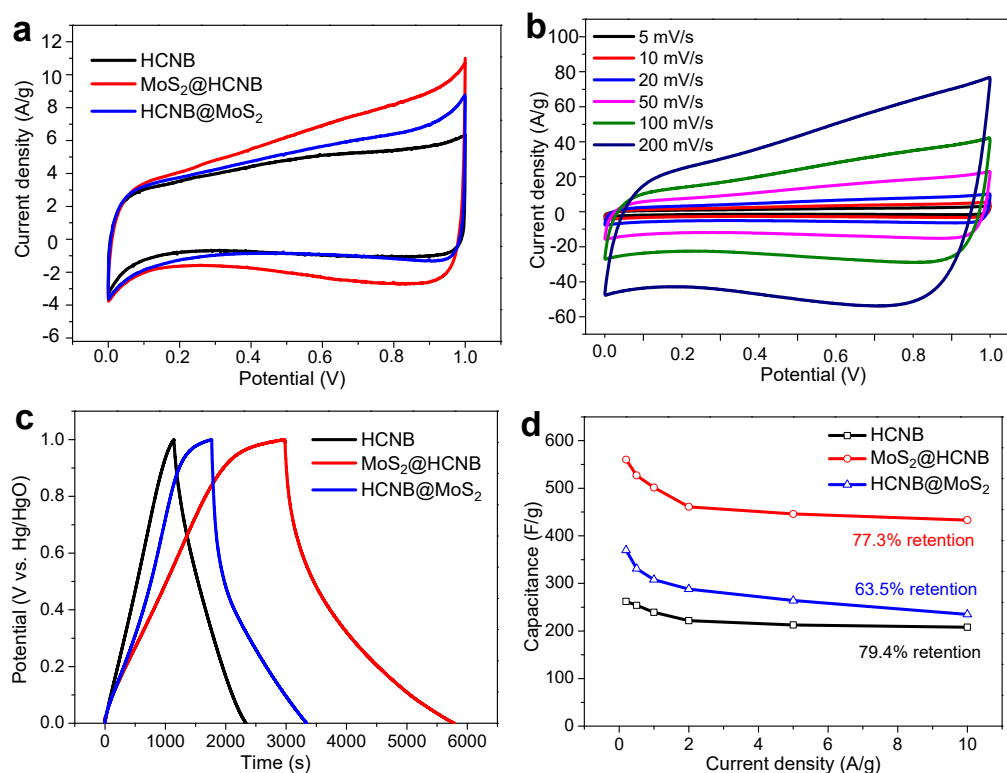
Fig. 5. (a) Cyclic Voltammetry (CV) curves tested at 5 mV s^{-1} for HCNB, MoS₂@HCNB and HCNB@MoS₂, (b) CV curves at the various scanning rates for MoS₂@HCNB, (c) Galvanostatic charge-discharge (GCD) curves measured at 0.2 A g^{-1} for HCNB, MoS₂@HCNB and HCNB@MoS₂; and (d) corresponding gravimetric capacitance versus discharge current density from 0.2 A g^{-1} to 10 A g^{-1}.
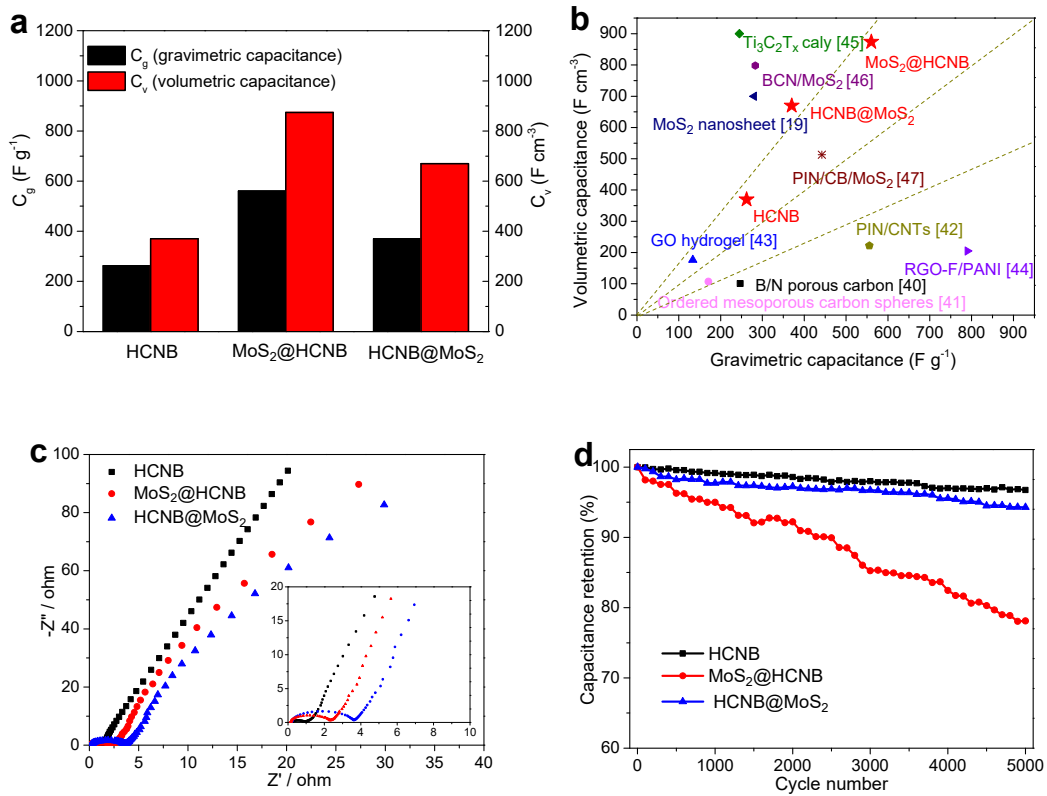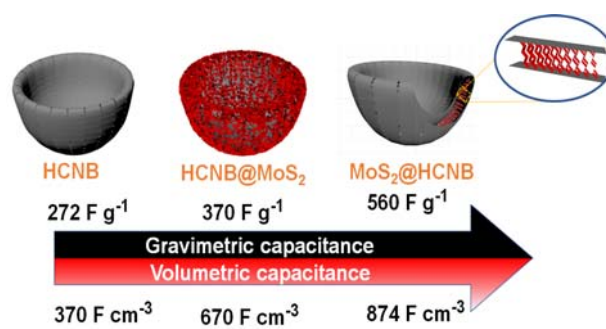
Fig. 6. (a) volumetric capacitances (C_v) vs. gravimetric capacitances (C_g) of HCNB, MoS$_2$@HCNB and HCNB@MoS$_2$, (b) C_v vs. C_g of the as-prepared electrode materials with previously reported related materials, (c) The Nyquist plot (the inset is the enlarged spectrum in the low impedance regime), and (d) cycling performance at 5.0 A g^{-1} for 5000 cycles.

Table of Contents Graphic

HCNB — 272 F g^{-1} — 370 F cm^{-3}

HCNB@MoS$_2$ — 370 F g^{-1} — 670 F cm^{-3}

MoS$_2$@HCNB — 560 F g^{-1} — 874 F cm^{-3}

Gravimetric capacitance

Volumetric capacitance

Supporting Information

Carbon Nano Bowls Filled with MoS$_2$ Nanosheets as Electrode Materials for Supercapacitors

*Lijian Wang [a], Fenghua Liu [a], Binyuan Zhao [a, *], Yuesheng Ning [a], Lifeng Zhang [b, *], Robert Bradley [c, d, e] and Weiping Wu [f,*]*

[a] State Key Laboratory of Metal Matrix Composites, School of Materials Science and Engineering, Shanghai Jiao Tong University, Shanghai, 200240, China

[b] School of Materials Science and Engineering, Shaanxi University of Science and Technology, Xi'an 710021, Shaanxi, China

[c] Department of Materials, University of Oxford, 16 Parks Road, Oxford, OX1 3PH, United Kingdom

[d] MatSurf Ltd, The Old Stables Marion Lodge, Little Salkeld, Penrith, Cumbria, CA10 1NW, United Kingdom

[e] School of Energy Resources, University of Wyoming, Laramie, WY, 82071, USA

[f] Department of Electrical and Electronic Engineering, School of Mathematics, Computer Science and Engineering, City, University of London, Northampton Square, London, EC1V 0HB, United Kingdom

f Department of Electrical and Electronic Engineering, School of Mathematics, Computer Science and Engineering, City, University of London, Northampton Square, London, EC1V 0HB, United Kingdom

*E-mail: byzhao@sjtu.edu.cn, zhanglifeng@sust.edu.cn, Weiping.Wu@city.ac.uk

Content:

1. Figure S1. TEM images of HCNB@MoS$_2$-1 and HCNB@MoS$_2$-3

2. Figure S2. TGA curves of HCNB, MoS$_2$@HCNB and HCNB@MoS$_2$

3. Figure S3. CV curves at the various scanning rates for HCNB and HCNB@MoS$_2$

4. Figure S4. GCD curves at the various scanning rates for HCNB, MoS$_2$@HCNB and HCNB@MoS$_2$

5. Figure S5. CV and GCD curves at the various scanning rates for HCNB@MoS$_2$ samples with different amount of MoS$_2$ wrapped on the surface of HCNB

6. Figure S6. A photograph of 100 mg of HCNB, MoS$_2$@HCNB and HCNB@MoS$_2$ tapped in quartz tubes

7. Figure S7. SEM characterizations of HCNB, MoS$_2$@HCNB and HCNB@MoS$_2$ electrodes after 5000 discharge/charge cycles at 5.0 A g^{-1}.

8. Figure S8. SEM images of the electrode thickness for HCNB, MoS$_2$@HCNB and HCNB@MoS$_2$ electrodes.

9. Textural parameters and compacting densities of HCNB, MoS$_2$@HCNB and HCNB@MoS$_2$

10. Elemental composition of HCNB, MoS$_2$@HCNB and HCNB@MoS$_2$ by XPS

11. Comparison of the as-prepared electrode materials with previously reported related materials

12. Estimation of the theoretical specific capacity of MoS$_2$
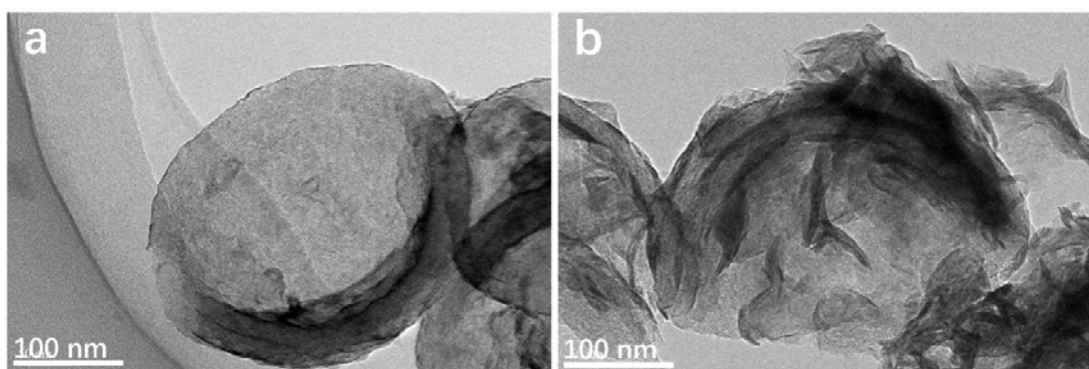
1. TEM images of HCNB@MoS$_2$-1 and HCNB@MoS$_2$-3

Figure S1. TEM images of (a) HCNB@MoS$_2$-1 and (b) HCNB@MoS$_2$-3

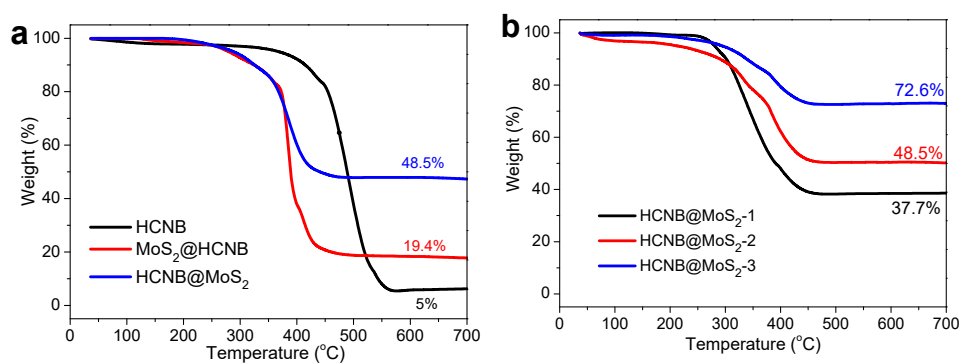# 2. TGA curves of HCNB, MoS$_2$@HCNB and HCNB@MoS$_2$

Figure S2. TGA curves of (a) HCNB, MoS$_2$@HCNB and HCNB@MoS$_2$ (This refers to HCNB@MoS$_2$-2), and (b) HCNB@MoS$_2$-1, HCNB@MoS$_2$-2 and (b) HCNB@MoS$_2$-3 which were synthesized by the solvothermal method with different concentrations of (NH4)$_2$MoS$_4$.

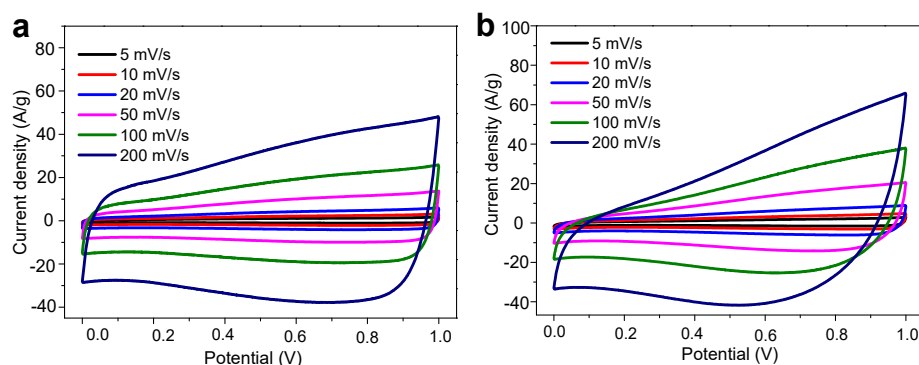## 3. CV curves at the various scanning rates for HCNB and HCNB@MoS₂

Figure S3. CV curves at the various scanning rates for (a) HCNB and (b) HCNB@MoS₂

4. GCD curves at the various scanning rates for HCNB, MoS₂@HCNB and HCNB@MoS₂

Figure S4. GCD curves (a-c) at the various scanning rates for (a) HCNB, (b) MoS₂@HCNB and (c) HCNB@MoS₂(HCNB@MoS₂-2).

5. CV and GCD curves at the various scanning rates for HCNB@MoS$_2$ samples with different amount of MoS$_2$ wrapped on the surface of HCNB
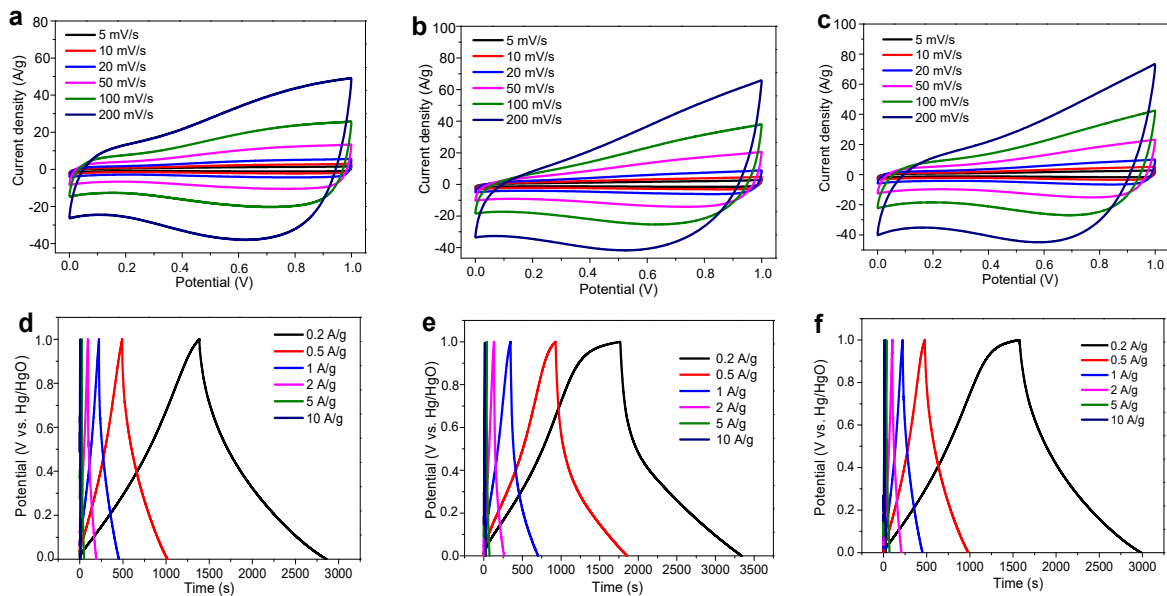

Figure S5. CV curves (a-c) at the various scanning rates for (a) HCNB@MoS$_2$-1, (b) HCNB@MoS$_2$-2 and (c) HCNB@MoS$_2$-3, and GCD curves at the various scanning rates for (d) HCNB@MoS$_2$-1, (e) HCNB@MoS$_2$-2 and (f) HCNB@MoS$_2$-3

6. A photograph of 100 mg of HCNB, MoS$_2$@HCNB and HCNB@MoS$_2$ tapped in quartz tubes

Figure S6. 100 mg HCNB, MoS$_2$@HCNB and HCNB@MoS$_2$ tapped in quartz tubes. The tap densities were evaluated by placing 100mg samples into a dry measuring cylinder, then taped hundreds of times[1]. Notably, HCNB with semi-concave structure is derived from the collapse of hollow spheres, which makes it can be densely stacked and has an enhanced packing density than other carbon electrode materials. In addition, MoS$_2$@HCNB, which confine the growth of ultra-small MoS$_2$ nanosheets within the HCNB, did not alter the backbone structure of the HCNB. Therefore, the MoS$_2$@HCNB is about 10% higher packing density (1.56 g cm^{-3}) than HCNB (1.41 g cm^{-3}).

7. SEM characterizations of HCNB, MoS₂@HCNB and HCNB@MoS₂ electrodes after 5000 discharge/charge cycles at 5.0 A g⁻¹.
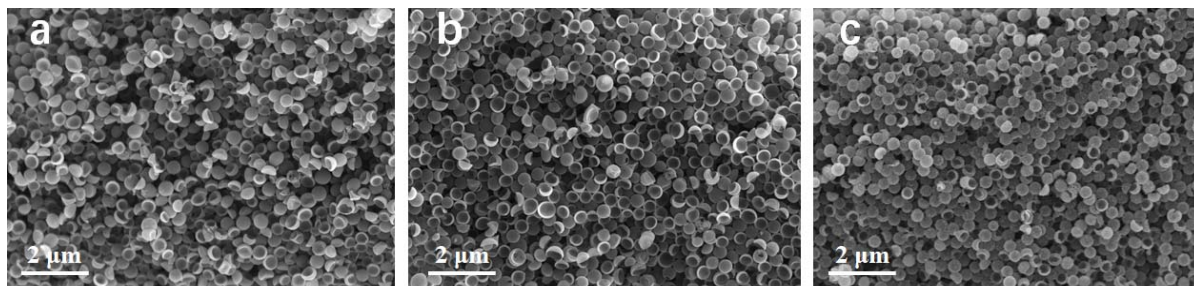

Figure S7. SEM images of (a) HCNB, (b) MoS₂@HCNB and (c) HCNB@MoS₂ electrodes after 5000 discharge/charge cycles at 5.0 A g⁻¹.

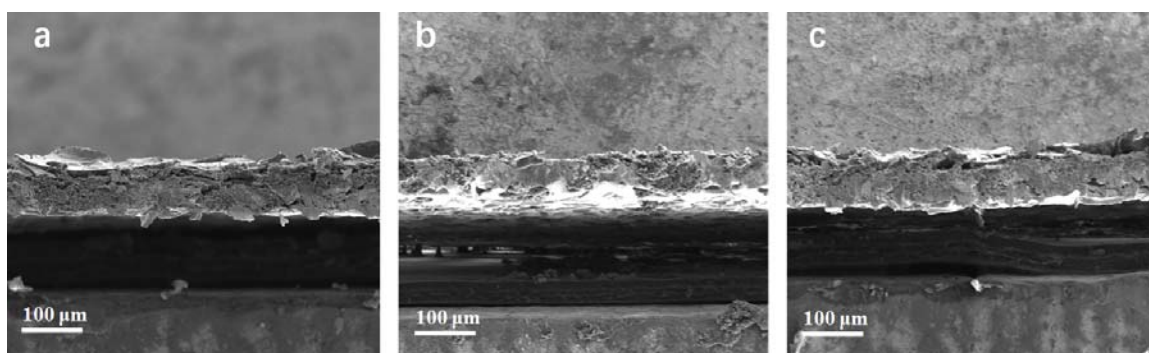**8. The electrode thickness of the HCNB, MoS₂@HCNB and HCNB@MoS₂ electrodes.**

Figure S8. SEM images of the electrode thickness for (a) HCNB, (b) MoS₂@HCNB and (c) HCNB@MoS₂ electrodes.

9. Textural parameters and compacting densities of HCNB, MoS_2@HCNB and HCNB@MoS_2

Table S1. Textural parameters and compacting densities of HCNB, MoS_2@HCNB and HCNB@MoS_2

Samples	N_2 adsorption-desorption			Packing density (g cm^{-3})
	S_{BET} (m^2 g^{-1})	pore width (nm)	V_{total} (cm^3 g^{-1})	
HCNB	1400.0	2.25	1.17	1.41
MoS_2@HCNB	734.8	2.15	0.70	1.56
HCNB@MoS_2	286.1	2.01	0.37	1.81

10. Elemental composition of HCNB, MoS_2@HCNB and HCNB@MoS_2 by XPS

Table S2. Elemental composition of HCNB, MoS_2@HCNB and HCNB@MoS_2 by XPS

Samples	C (at%)	N (at%)	O (at%)	S (at%)	Mo (at%)
HCNB	91.0	3.6	5.4	—	—
MoS_2@HCNB	68.5	12.4	14.8	2.3	1.0
HCNB@MoS_2	59.2	11.6	14.9	7.0	3.4

11. Comparison of the as-prepared electrode materials with previously reported materials

Table S3. Comparison of the as-prepared electrode materials with previously reported materials

Materials	C_g (F g^{-1})	C_v (F cm^{-3})	Scan rate	Electrolytes	Ref
B/N porous carbon	247	101	0.50 A g^{-1}	6M KOH	2
Carbon nanosheets	233	177	0.1 A g^{-1}	1M H$_2$SO$_4$	3
Ordered mesoporous carbon	171	107	5 mV·s^{-1}	6M KOH	4
CNFs	280	88	0.50 A g^{-1}	6M KOH	5
RGO	285	218	1 A g^{-1}	6M KOH	6
RGO film	180	226	5 mV s^{-1}	6M KOH	7
3D porous carbon	318	118	0.50 A g^{-1}	6M KOH	8
GO hydrogel	133.6	176.5	1 A g^{-1}	6M KOH	9
Holey GF	208	148	1 A g^{-1}	6M KOH	10
Ti$_3$C$_2$T$_x$ clay	245	900	2 mV s^{-1}	1 M H$_2$SO$_4$	11
2H-MoS$_2$ nanosheet	280	700	5 mV s^{-1}	0.5 M H$_2$SO$_4$	12
RGO-F/PANI	790	205	1 A g^{-1}	1 M H$_2$SO$_4$	13
PANI/graphene	546	802	0.1 A g^{-1}	1 M H$_2$SO$_4$	14
aMEGO/MnO$_2$	256	640	0.5 A g^{-1}	1 M H$_2$SO$_4$	15
BCN/MoS$_2$	283	798	1 A g^{-1}	1 M H$_2$SO$_4$	16
PIn/CB/MoS$_2$	442	512.7	1 A g^{-1}	1 M H$_2$SO$_4$	17
PIN/CNTs	555.6	222.2	0.5 A g^{-1}	1 M H$_2$SO$_4$	18
HCNB	**272**	**370**	**0.2 A g^{-1}**	**6M KOH**	**This work**
HCNB@MoS$_2$	**370**	**670**	**0.2 A g^{-1}**	**6M KOH**	**This work**
MoS$_2$@HCNB	**560**	**874**	**0.2 A g^{-1}**	**6M KOH**	**This work**

12. Estimation of the theoretical specific capacity of Molybdenum disulfide (MoS$_2$)

Molybdenum disulfide (MoS$_2$) has relatively high theoretical specific capacity as the electrode material for supercapacitors. The theoretical specific capacity (Cs) of MoS$_2$ can be calculated according to the following formula[19],

$$C_s = \frac{n \times F}{m \times V}$$

Where n is the electron number, F is the Faraday constant (96,485 C mol^{-1}), m is the molecular weight, V is the redox potential.

The pseudocapacitance of MoS$_2$ is due to the faradaic charge transfer of Mo during the electrochemical process, in which Mo could show several oxidation states from +2 to +6, so it can show a pseudocapacitor similar to RuO$_2$. The redox reactions of Mo4+ in aqueous electrolyte generally gains or loses 2 electrons. Therefore, the total number of electrons taking part in the reaction, $n = 2$.

Therefore, the theoretical specific capacity of MoS$_2$ is calculated as 1200 F g^{-1}.

REFERENCES

(1) Zhang, Z. L.; Qin, M. L.; Jia, B. R.; Zhang, H. Z.; Wu, H. Y.; Qu, X. H. Facile Synthesis of Novel Bowl-Like Hollow Carbon Spheres by the Combination of Hydrothermal Carbonization and Soft Templating. *Chem. Commun.* **2017**, 53, 2922–2925.

(2) Guo, D. C.; Mi, J.; Hao, G. P.; Dong, W.; Xiong, G.; Li, W. C.; Lu, A. H. Ionic Liquid C_{16}mimBF$_4$ Assisted Synthesis of Poly(Benzoxazine-Co-Resol)-Based Hierarchically Porous Carbons with Superior Performance in Supercapacitors. *Energy Environ. Sci* **2013**, 6, 652–659.

(3) Ling, Z.; Wang, Z. Y.; Zhang, M. D.; Yu, C.; Wang, G.; Dong, Y. F.; Liu, S. H.; Wang, Y. W.; Qiu, J. S. Sustainable Synthesis and Assembly of Biomass-Derived B/N Co-Doped Carbon Nanosheets with Ultrahigh Aspect Ratio for High-Performance Supercapacitors. *Adv. Funct. Mater.* **2016**, 26, 111–119.

(4) Yu, X. L.; Wang, J. G.; Huang, Z. H.; Shen, W. C.; Kang, F. Y. Ordered Mesoporous Carbon Nanospheres as Electrode Materials for High-Performance Supercapacitors. *Electrochem Commun* **2013**, 36, 66–70.

(5) Li, W.; Zhang, F.; Dou, Y. Q.; Wu, Z. X.; Liu, H. J.; Qian, X. F.; Gu, D.; Xia, Y. Y.; Tu, B.; Zhao, D. Y., A Self-Template Strategy for the Synthesis of Mesoporous Carbon Nanofibers as Advanced Supercapacitor Electrodes. *Adv. Energy Mater.* **2011**, 1, 382–386.

(6) She, Z.; Ghosh, D.; Pope, M. A. Decorating Graphene Oxide with Ionic Liquid Nanodroplets: An Approach Leading to Energy-Dense, High-Voltage Supercapacitors. *ACS Nano* **2017**, 11, 10077–10087.

(7) Jiang, L. L.; Sheng, L. Z.; Long, C. L.; Fan, Z. J. Densely Packed Graphene Nanomesh-Carbon Nanotube Hybrid Film for Ultra-High Volumetric Performance Supercapacitors. *Nano Energy* **2015**, 11, 471–480.

(8) Qie, L.; Chen, W. M.; Xu, H. H.; Xiong, X. Q.; Jiang, Y.; Zou, F.; Hu, X. L.; Xin, Y.; Zhang, Z. L.; Huang, Y. H. Synthesis of Functionalized 3D Hierarchical Porous Carbon for High-Performance Supercapacitors. *Energy Environ. Sci.* **2013**, 6, 2497–2504.

(9) Pham, V. H.; Dickerson, J. H. Reduced Graphene Oxide Hydrogels Deposited in Nickel Foam for Supercapacitor Applications: Toward High Volumetric Capacitance. *J. Phys. Chem. C* **2016**, 120, 5353–5360.

(10) Xu, Y. X.; Lin, Z. Y.; Zhong, X.; Huang, X. Q.; Weiss, N. O.; Huang, Y.; Duan, X. F. Holey Graphene Frameworks for Highly Efficient Capacitive Energy Storage. *Nat. Commun.* **2014**, 5, 4554.

(11) Ghidiu, M.; Lukatskaya, M. R.; Zhao, M. Q.; Gogotsi, Y.; Barsoum, M. W. Conductive Two-Dimensional Titanium Carbide 'Clay' with High Volumetric Capacitance. *Nature* **2014**, 516, 78–81.

(12) Acerce, M.; Voiry, D.; Chhowalla, M. Metallic 1T Phase MoS_2 Nanosheets as Supercapacitor Electrode Materials. *Nat. Nanotechnol.* **2015**, 10, 313–318.

(13) Yu, P. P.; Zhao, X.; Huang, Z. L.; Li, Y. Z.; Zhang, Q. H. Free-Standing Three-Dimensional Graphene and Polyaniline Nanowire Arrays Hybrid Foams for High-Performance Flexible and Lightweight Supercapacitors. *J. Mater. Chem. A* **2014**, 2, 14413–14420.

(14) Xu, Y.; Tao, Y.; Zheng, X. Y.; Ma, H. Y.; Luo, J. Y.; Kang, F. Y.; Yang, Q. H. A Metal-Free Supercapacitor Electrode Material with a Record High Volumetric Capacitance over 800 F cm^{-3}. *Adv. Mater.* **2015**, 27, 8082–8087.

(15) Zhao, X.; Zhang, L. L.; Murali, S.; Stoller, M. D.; Zhang, Q. H.; Zhu, Y. W.; Ruoff, R. S. Incorporation of Manganese Dioxide within Ultraporous Activated Graphene for High-Performance Electrochemical Capacitors. *ACS Nano* **2012**, 6, 5404–5412.

(16) Thakur, A. K.; Majumder, M.; Choudhary, R. B.; Singh, S. B. MoS_2 Flakes Integrated with Boron and Nitrogen-Doped Carbon: Striking Gravimetric and Volumetric Capacitive Performance for Supercapacitor Applications. *J. Power Sources* **2018**, 402, 163–173.

(17) Majumder, M.; Choudhary, R. B.; Koiry, S. P.; Thakur, A. K.; Kumar, U. Gravimetric and Volumetric Capacitive Performance of Polyindole/Carbon Black/MoS_2 Hybrid Electrode Material for Supercapacitor Applications. *Electrochim. Acta* **2017**, 248, 98–111.

(18) Cai, Z. J.; Zhang, Q.; Song, X. Y. Improved Electrochemical Performance of Polyindole/Carbon Nanotubes Composite as Electrode Material for Supercapacitors. *Electron. Mater. Lett.* **2016**, 12, 830–840.

(19) Krishnan, S. G.; Reddy, M. V.; Harilal, M.; Vidyadharan, B.; Misnon, I. I.; Ab Rahim, M. H.; Ismail, J.; Jose, R. Characterization of $MgCo_2O_4$ as an Electrode for High Performance Supercapacitors. *Electrochim. Acta* **2015**, 161, 312–321.